HHS Public Access

Author manuscript

J Mater Res. Author manuscript; available in PMC 2019 February 08.

Published in final edited form as:

J Mater Res. 2018 ; 33(14): 1939–1947. doi:10.1557/jmr.2018.233.

3D printed β-TCP bone tissue engineering scaffolds: Effects of chemistry on *in vivo* biological properties in a rabbit tibia model

Samit Kumar Nandi[2], **Gary Fielding**[1], **Dishary Banerjee**[1], **Amit Bandyopadhyay**[1], and **Susmita Bose**[1]

[1]W. M. Keck Biomedical Materials Research Laboratory, School of Mechanical and Materials Engineering, Washington State University, Pullman, WA 99164-2920, USA

[2]Department of Veterinary Surgery and Radiology, West Bengal University of Animal and Fishery Sciences, India

Abstract

In this study the effects of 3D printed SiO_2 and ZnO doped tricalcium phosphate (TCP) scaffolds with interconnected pores were evaluated on the *in vivo* bone formation and healing properties of a rabbit tibial defect model. Pure and doped TCP scaffolds were fabricated by a ceramic powder-based 3D printing technique and implanted into critical sized rabbit tibial defects for up to 4 months. *In vivo* bone regeneration was evaluated using chronological radiological examination, histological evaluations, SEM micrographs and fluorochrome labeling studies. Radiograph results showed that Si/Zn doped samples had slower degradation kinetics than the pure TCP samples. 3D printing of TCP scaffolds improved bone formation. The addition of dopants in the TCP scaffolds improved osteogenic capabilities when compared to the pure scaffolds. In summary, our findings indicate that addition of dopants to the TCP scaffolds enhanced bone formation and in turn leading to accelerated healing.

Graphical Abstract

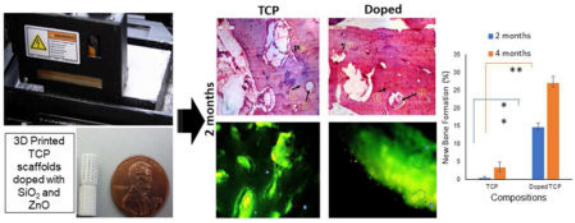

Keywords

biomaterials; bone; ceramic

Phone: 1-(509) 335-7461, Fax: 1-(509) 335-4662 1, sbose@wsu.edu.

1. Introduction

The development of materials mimicking functional and structural characteristics of natural tissues still poses a challenge, despite significant efforts from the scientific community. Over the past few decades, bioceramics have emerged as a viable material candidate for orthopedic, maxillofacial, and dental applications [1]. Amidst various ceramic materials that have been explored for *in vivo* implantation, calcium phosphate (CaP) materials, especially β-tricalcium phosphate (β-TCP) have found widespread usage in non/low load bearing orthopedic implant applications due to their compositional similarity to natural bone, inherent osteoconductivity and tailorable bioresorbability [1–3]. However, they have demonstrated limited ability to stimulate cellular differentiation and bone regeneration on their own [3,4].

An ideal scaffold utilized for bone healing should have optimized density, pore size, pore shape and interconnectivity to support tissue ingrowth and mechanical amalgamation at bone-implant interface [5]. Since natural bone is inherently porous with interconnected pores, research has been devoted towards the fabrication of porous ceramic scaffolds. The presence of macro-porosity facilitates nutrient exchange and waste removal process leading to induction of enhanced bone formation and improvement in functional activities of the tissue [6]. Moreover, reports suggest an optimal pore diameter of 300 to 500 μms for improved osteogenesis and angiogenesis [7–8]. Manufacturing of porous ceramic scaffolds using conventional techniques is limited by the precision required over the pore size, shape and geometry. 3D printing makes it feasible to fabricate ceramic scaffolds for bone graft applications taking into account unusual injury and anatomy. It also has the inherent advantages of generating macro-porosity within the scaffold during the fabrication process without the need for a support structure, eliminating multiple post processing steps and preparation of patient/defect specific implants [6]. Previous works from our group have reported the use of the 3D printed scaffolds for the study of biological and mechanical properties in a rat distal femur model [6]. In this study, we have fabricated 3D printed β-TCP scaffolds 7 mm by 10.5 mm to evaluate their biological and mechanical properties in a rabbit model.

One of the major challenges involved in implantation of porous ceramic scaffolds are their low strength, especially at high volume percentage of porosity [6]. Synthesis of cation-substituted TCP ceramic scaffolds is becoming a major thrust area due to the crucial role of ions in the biological activity of bone [2,9–11]. It has been demonstrated that trace element incorporation in TCP powder as dopants can effectively control the resorption rates, densification, cell–material interactions and mechanical properties [2,12]. Silicon has been long associated with structural stabilization of collagen and enhanced bone mineral density [13–14]. Studies have also reported improved angiogenesis with silica incorporation in TCP scaffolds [2,15]. Addition of ZnO, on the other hand, can effectively control grain growth, increase density and stimulate bone formation *in vitro* and *in vivo* in a rat distal femur model [15]. It has been shown to inhibit osteoclastic bone resorption and induce apoptosis of mature osteoclasts [15–17].

The combined effects of SiO_2 and ZnO have never been studied on the osteogenic and angiogenic properties *in vivo* in a rabbit tibia defect model. Thus, it is important to investigate whether the 3D printed porous doped TCP scaffolds can induce faster bone regeneration in an *in vivo* environment and whether the degradation rate of scaffolds is sufficient enough to provide the temporary support structure necessary for complete healing of a critical sized defect. In the present study, we have developed silica (SiO_2) and zinc oxide (ZnO) doped 3D interconnected porous TCP scaffolds to evaluate their *in vivo* performance in a rabbit critical sized tibial defect model on bone regeneration.

2. Materials and methods

2.1. Fabrication of porous scaffold

Commercially pure β-tricalcium phosphate (β-TCP), average particle size 550 nm, was purchased from Berkeley Advanced Biomaterials, CA, USA. 0.5 wt % SiO_2 and 0.25 wt % of ZnO were mixed thoroughly with 50 g of β-TCP powder in a nalgene bottle containing 75 ml of anhydrous ethanol and 100 g of zirconia milling media for 2 h at 70 rpm and dried at 60°C in an oven for 72 hours [15]. Scaffolds, 7 mm in diameter and 10.5 mm in height were developed in a CAD file and fed into a ceramic powder-based binder-jet 3D printer (ProMetal, ExONE LLC, Irwin, PA, USA). Interconnected pores 500 μm were designed to be square in shape and distributed throughout in X, Y and Z directions. Layer thickness was optimized to be 20 μm and other parameters for the 3D printing process like saturation, binder drop volume and drying time was optimized for the building process [6]. The green fabricated scaffolds were depowderized using an air blower, cured at 175°C for 1.5 hrs and sintered in a conventional muffle furnace at 1250°C for 2 h and cooled to room temperature. Figure 1(a) represents the schematic 3D printing process.

2.2. Microstructure and mechanical properties

Screw-driven universal testing machine (AG-IS, Shimadzu, Japan) with a constant crosshead speed of 0.33 mm/min was utilized to evaluate the compressive strength of the fabricated scaffolds, ten replicates for each composition. The recorded compressive strengths were calculated from the maximum load borne and the dimensions of the sintered scaffolds. The surface morphologies of the sintered scaffolds were demonstrated by a field emission scanning electron microscope (FESEM) (FEI Inc., OR, USA).

2.3. *In vivo* study

In vivo experiments were conducted in the Department of Veterinary Surgery and Radiology, West Bengal University of Animal and Fishery Sciences, India in compliance with Institutional Animal Ethical Committee of the University. Skeletally mature New Zealand white male rabbits, weighing 2–2.5 kg, were used in this study. The animals were housed individually and supplied with consistent balanced standard diet along with ample supply of water, in an identical management and environment. After routine pre-operative drug administration, the rabbits were anaesthetized using approved combination of xylazine hydrochloride (1 mg/kg body weight; Indian Immunologicals, Hyderabad, India) and ketamine hydrochloride (11 mg/kg body weight; Ketalar®, Parke-Davis, Hyderabad, India). A 2 cm longitudinal skin incision was made on the medial side of the tibia bone in both the

limbs and critical sized bone defects were created by micromotor dental drill in both the tibia under aseptic conditions. Each animal was implanted with SiO_2/ZnO doped TCP scaffold and pure TCP scaffold following an unbalanced completely random statistical design (Figure 2). Implants were secured in position by suturing muscle, subcutaneous tissue, and skin in layers. After suturing, the animals were administered cefotaxime sodium injection (125 mg intramuscularly twice daily, Mapra India, Kolkata, India) and meloxicam injection (0.2 ml intramuscularly once daily for 5 days Intas Pharmaceuticals, Ahmedabad, India) for subsidizing pain. Surgical wounds were dressed daily with iodine and antibiotic cream for 5 days postoperatively. Animals were sacrificed at 2 months and 4 months after implantation to assess and compare the progressive bone formation and healing potentialities.

2.4. Histological analysis

For histological investigation, osseous tissue specimens containing the implant were excised 2 and 4 months after euthanization postoperatively and washed thoroughly with normal saline and were fixed in 10% neutral buffered formalin for 7 days. Decalcification was carried out in Goodling and Stewart's fluid containing 15% formic acid and 5% formalin in DI water for around 8 weeks. Further, after serial dehydration in ethanol, the tissue specimens embedded in paraffin wax. 4 μm sections were cut out using a microtome cutter and stained with hematoxylin and eosin (H&E) to observe the osteogenic properties of the implants and cellular response at the host bone and implant interface.

2.5. Field emission scanning electron microscopic (FESEM) analysis

Following removal of soft tissues, the osseous tissues were fixed in 5% glutaraldehyde phosphate solution. After washing with neutral phosphate buffer and DI water twice for 30 mins and series dehydration with anhydrous ethanol and hexamethyldisilane, the specimens were covered with a gold conductive coating (JEOL ion sputter, model JFC 1100, Japan) at 7–10 mA and 1–2 kV for 5 min). The surfaces were then observed under FESEM (FEI Inc., OR, USA) to examine distribution of newly formed osseous tissues and the bone-material interaction at the defect site.

2.6. Radiological observation

Radiographs images were taken (300 mA medical diagnostic X-ray machine, M.E. X-Ray, India) immediately after implantation (referred as day 0) and subsequently on days 30, 60, 90 and 120 of both the operated limbs to demonstrate bone-material interface, evaluate the degradation of the scaffolds over the function of time and observe the changes in radiopacity of the implants over time.

2.7. Fluorochrome labeling study

Fluorochrome labeling studies were carried out by injecting oxytetracycline dehydrate (Pfizer India) intramuscularly, at a dose rate 25 mg/kg body weight on days 48, 49 and after a 6-day interval on days 55 and 56 (2–6–2). The same 2-6-2 dosing was used for the 4-month time point at days 107, 108 and 115, 116 for double toning of new bone formation. After euthanizing, the implanted bone specimens were collected. The tissue sections were

further grounded to 20 mm thickness and observed under ultravioletincidental light with an Orthoplan microscope (Excitation filter, BP-400 range; Leitz, USA) for tetracycline labeling to examine the new bone formation. GNU Image Manipulation Program (GIMP) was utilized to quantitatively evaluate the new and old bone formation from the histology micrographs.

3. Results

3.1. Mechanical characterization

Addition of dopants into TCP increased the average density of pure TCP from 90.8 ± 0.8% to 94.1 ± 1.6% and compressive strengths from 5.48 ± 0.04 MPa to 10.21 ± 0.11 MPa. More densification due to the presence of dopants was attributed for improved mechanical properties. Figure 3 demonstrates the surface morphologies of the scaffolds sintered at 1250 °C. Interconnected pores has been observed and the sintered pore diameter was observed to be ranging from 350 μm to 380 μm after sintering. Both the pure and doped samples contain residual porosity. The SiO_2/ZnO doped samples appeared to undergo a high degree of liquid phase sintering evidenced by smooth, flowing grain structures.

3.2. Histological analysis

Histological evaluation (Figure 4) at the bone-implant interface was performed by H&E staining at 2 and 4 months after implantation to study the influence of SiO_2/ZnO on biocompatibility and new bone formation. Figure 4a depicts pure TCP scaffolds, showing moderate fibro-collagenization with normal osteoblastic proliferation whereas Figure 4b demonstrates doped TCP scaffolds, showing moderately differentiated lamellar bone in the cortical region and woven bone in peripheral regions with evidence of angiogenesis (cherry-red color). As shown in Figure 4c, the pure TCP scaffolds present moderate proliferation of osteoblastic and osteoclastic tissue, with instances of angiogenesis surrounding the harversian canals. At the same time point, the doped TCP scaffolds depicted intense fibro-osteoid proliferations around the harversian canals and lacunae along with enhanced osteoblastic activity and vascularization (Figure 4d).

3.3. SEM observation

Pure TCP scaffolds showed good osseous tissue bonding, with notable gaps at the bone-implant interface (Figure 5). The doped samples, however, showed nearly complete bone integration of mineralized tissue by 2 months. After 4 months, the pure TCP samples had nearly complete infiltration of mineralized tissue, while the doped samples were becoming increasingly more difficult to distinguish from natural bone. Signs of degradation were evident from doped scaffolds after 4 months of implantation with tuned in osseous tissue integration. These results indicate increased affinity towards new bone growth for the scaffolds containing SiO_2/ZnO dopants.

3.4. Radiological analysis

Radiological observations of the implants (Figure 6) at day 0 revealed the TCP scaffolds as radio dense materials in a rectangular defect of the proximal tibia with a zone of radiolucency surrounding the implant indicating the surgical defect. On day 30, the

radiographs indicated slight secondary osteophytic changes in distal part of the pure implant with substantial reduction of the radiolucent gap in both the pure TCP and Si/Zn doped TCP grafts between bone and implant indicating tissue regeneration at the defect sites. By day 60, the surgical defect site implanted with the Si/Zn TCP scaffolds showed nearly complete healing, while the site implanted with the pure TCP scaffold still had substantial radiolucent gaps. After 90 days implantation, results demonstrated a decrease in the radiodensity of the pure implant indicating a trend towards increased dissolution when compared to the Si/Zn TCP implants at the same time point. By day 120, the defect sites containing the pure TCP scaffolds showed complete healing and also demonstrated radiopacity more similar to the natural bone, while the Si/Zn scaffold still had substantially higher radiodensity, indicating a continued trend towards decreased dissolution rates of the doped samples.

3.5. Fluorochrome labeling study

Figure 7 shows fluorochrome labeling images, presenting new bone formation stained by golden yellow fluorescence, whereas sea-green color represents mature or old bone. Figure 7a imparted a double tone golden yellow fluorescence in the narrow zone in the implanted site, whereas the doped scaffolds showed more new bone formation originating from the host bone towards the implanted area as evidenced by golden yellow fluorescence (figure 7b). In both scaffolds, the intensity of new bone formation was more in the periosteal side than endosteal side. As shown in Figure 7c, pure TCP samples after 4 months had only moderate amounts of new bone formation observed, while doped scaffolds showed higher amounts of new bone formation (Figure 7d). The visual histological micrographs are more substantiated by the quantitative evaluation of old and new bone formation by GIMP, demonstrated in Figure 7e and 7f.

4. Discussion

β-TCP is considered to be an important bone graft material in clinical use due to its solubility, excellent biocompatibility, osteoconductivity and ability to provide a temporary framework for bone remodeling [18–20]. However, the use of β-TCP is limited by its inherent lack of osteoinductivity, the ability to induce new bone formation. One of the most commonly adopted procedures to integrate osteoinductivity in calcium phosphate scaffolds is by incorporation of bone derived growth factors like BMP-2, IGF-1 & 2, VGEF etc. [21,22]. However, it is necessary to ensure a sustained and controlled release of these growth factors from the scaffold and also, long term viability of these protein poses as a major challenge in scaffold incorporation [22]. Inclusion of cationic dopants in TCP scaffolds has been researched extensively for inducing osteoinductivity in an effort of overcoming the challenges associated with incorporation of growth factors [23]. Sintering additives with CaP materials has been investigated in the past to improve densification and in turn the mechanical strength of the material [24]. Demonstration of surface morphologies by SEM micrographs (Figure 3) indicates that SiO_2 and ZnO dopants may have the ability to shift the liquidus phase temperature of TCP. This is likely due to lattice imperfections arising from Si^{4+} and Zn^{2+} substitutions in the crystal structure [23–25]. Liquid phase sintering can lead to greater wettability during sintering, and in turn, increase the densification process by increasing capillary action and allowing for more efficient particle rearrangement [25].

Increased density of the doped samples, as a result of α-phase formation impedance and lowering of liquids phase temperature, ultimately is what caused the increase in the compressive strength of the scaffolds.

Histology micrographs for pure TCP (Figure 4) after 2 months show moderate fibro-collagenization and bony lamellae along with harversian systems. The osteoblastic and osteophytic proliferations are normal with well-defined periosteum, Volkmann's canals and fibrous tissue proliferation of bony stroma in the lacunae indicating normal histogenesis of bone. Doped TCP scaffolds at the same time point show moderately differentiated lamellar bone in the cortical region and woven bone in peripheral regions with evidences of angiogenesis in marrow spaces suggesting a further developed healing process than the pure TCP scaffolds. Similar observations of bone formation had been previously demonstrated with MgO/SrO doped β-TCP scaffolds by our group [2]. After 4 months of implantation time, the pure TCP scaffolds show moderate proliferation of osteoblastic tissue similar to the doped ones after 2 months of implantation. Vascular cells surrounded the harversian canal and showed normal fibrovascular patterns indicating normal regenerative process of bone. Doped scaffolds, 4 months after implantation, further depict intense fibro-osteoid proliferations around the harversian canal/lacunae along with extensive bone formation and angiogenesis indicating accelerated healing progress [26–29]. The increased bone formation in the doped scaffold [30–33] has been attributed to the stimulatory effects of the combination of zinc and silicon on bone formation [14, 15, 26, 30, 31].

Surface microstructural studies through SEM (Figure 5) demonstrated the presence of an interfacial gap with moderately developed tissue ingrowth into the porous structure of pure TCP scaffolds after 2 months. The doped scaffolds had enhanced osseointegration at the bone-implant interface compared to the control [34]. The presence of no interfacial gap between the material and the bone at 4 months' time point in doped specimens, along with increased osteoblastic activities, suggested better bone-implant bonding when compared to the pure TCP samples. This is likely due to the transformation of the implanted material to a more biological-like apatite and the stimulation of the osteoblastic activity due to the presence of the SiO_2 and ZnO dopants [14–15]. The characteristic osteoblastic cell was noticed over the surface of the implanted material indicating faster bone regeneration which corroborated the findings using a rat distal femur model [22].

Radiography is an excellent tool used in orthopedic biomaterials to assess the mechanical interlocking at the host bone-implant interface *in vivo* [35], along with valuable insights into degradation kinetics of the implanted scaffolds by examination of the relative changes in radiodensity [36]. A distinct radiolucent zone was noted on the immediate postoperative radiographs at the interface of the scaffolds immediately after surgery (Figure 6). The gradual absence of this zone is considered to be an indication of improved interfacial bone tissue integration [37]. In pure TCP scaffolds the radiodensity of the implant was comparable to the host bone on day 120 suggesting the initiation of resorption of implant by formation of hard tissue within the defect area and reparative phase. In the doped specimens, more rapid disappearance of gap was observed, which initiated as early as on day 30 and completely disappeared by day 90 indicating a rapid healing process. The Si/Zn TCP implants also retained lower radiopacity over the course of the study, indicating a slower

dissolution rate leading to enhanced support for bone regeneration. Slower degradation kinetics were also shown by 3D printed $MgO/SiO_2/SrO$ doped scaffolds in simulated body fluid (SBF) at pH 7.4 [2].

New and old bone formation around the area of implantation was further quantified by tetracycline labeling and fluorescence studies. Tetracycline actively trails the ionized calcium ion in the blood and gets absorbed during bone mineralization [36–37]. Under UV light, the old bone is depicted as sea green color, whereas the newly formed osseous tissue emits a bright golden yellow color. Tetracycline labeling micrographs (Figure 7) confirmed enhanced new bone formation in the doped scaffolds. More new bone formation was demonstrated on periosteal surface than endosteal surface. 4 months after implantation, the defects implanted with doped scaffolds were filled with newly formed bone as demonstrated by the homogenous golden yellow areas, suggesting a positive influence on new bone growth using silicon and zinc dopants [30–31]. These results are further substantiated by the quantitative histomorphometric analyses performed from the micrographs using GIMP.

Collectively, our results reveal that SiO_2/ZnO doped TCP can enhance early stages of bone formation and implant fixation when compared to pure TCP alone in a rabbit tibia model. Slow degradation of SiO_2/ZnO doped TCP, suggested by radiographs, demonstrate higher scaffold stability *in vivo*, leading to longer temporary support for bone regeneration. Moreover, the presence of designed interconnected porosity facilitates waste removal and enhances nutrient movements leading to improved bone tissue and implants interlocking and evidences of blood vessel formation *in vivo*.

Conclusion

This study examined the influence of SiO_2 and ZnO dopants in 3D printed TCP scaffolds, with interconnected porosity on *in vivo* biological performance over the course of 4 months in a rabbit tibia defect model. The presence of dopants revealed higher densification compared to the pure TCP ones, eventually leading to improved mechanical strength. Our radiographs indicated a slower degradation kinetics of the doped scaffolds compared to the pure TCP ones, thus providing longer support for bone regeneration. SEM micrographs and histology images suggested enhanced new bone formation in doped scaffolds and strong osseous tissue interlocking into the macro pores of the scaffolds and were substantiated by quantitative histomorphometric analysis. After 4 weeks of implantation, histology images also suggested evidences of angiogenesis, facilitated by enhanced nutrient exchange and waste removal through the interconnected pores. These findings suggest that the incorporation of SiO_2 and ZnO as dopants into porous 3D printed TCP scaffolds have the potential to be translated in clinical settings for rapid bone regeneration and hence, accelerated healing.

Acknowledgments

Authors would like to acknowledge financial support from the National Institutes of Health (Grant # NIH-R01-AR-006361). The authors wish to acknowledge the help rendered by Dr. Solaiman Tarafder, Washington State University and Vice Chancellor, West Bengal University of Animal and Fishery Sciences, Kolkata, India for their generous and kind support to this work.

References

1. Bandyopadhyay A, Bernard S, Xue W, Bose S. Calcium Phosphate-Based Resorbable Ceramics: Influence of MgO, ZnO, and SiO2 Dopants. Journal of the American Ceramic Society. 89(9):2675–2688.2006;
2. Bose S, Tarafder S, Banerjee SS, Davies NM, Bandyopadhyay A. Understanding in vivo response and mechanical property variation in MgO, SrO and SiO2 doped β-TCP. Bone. 48(6):1282–1290.2011; [PubMed: 21419884]
3. Liu Q, Cen L, Yin S, Chen L, Liu G, Chang J, Cui L. A comparative study of proliferation and osteogenic differentiation of adipose-derived stem cells on akermanite and β-TCP ceramics. Biomaterials. 29(36):4792–4799.2008; [PubMed: 18823660]
4. Huang Y, Jin X, Zhang X, Sun H, Tu J, Tang T, Chang J, Dai K. In vitro and in vivo evaluation of akermanite bioceramics for bone regeneration. Biomaterials. 30(28):5041–5048.2009; [PubMed: 19545889]
5. Hutmacher DW. Scaffolds in tissue engineering bone and cartilage. The Biomaterials: Silver Jubilee Compendium. :175–189.2006
6. Tarafder S, Balla VK, Davies NM, Bandyopadhyay A, Bose S. Microwave-sintered 3D printed tricalcium phosphate scaffolds for bone tissue engineering. Journal of tissue engineering and regenerative medicine. 7(8):631–641.2013; [PubMed: 22396130]
7. Karageorgiou V, Kaplan D. Porosity of 3D biomaterial scaffolds and osteogenesis. Biomaterials. 26(27):5474–5491.2005; [PubMed: 15860204]
8. Otsuki B, Takemoto M, Fujibayashi S, Neo M, Kokubo T, Nakamura T. Pore throat size and connectivity determine bone and tissue ingrowth into porous implants: three-dimensional micro-CT based structural analyses of porous bioactive titanium implants. Biomaterials. 27(35):5892–5900.2006; [PubMed: 16945409]
9. Bohner M, Loosli Y, Baroud G, Lacroix D. Commentary: deciphering the link between architecture and biological response of a bone graft substitute. Acta biomaterialia. 7(2):478–484.2011; [PubMed: 20709195]
10. Bohner M, Baumgart F. Theoretical model to determine the effects of geometrical factors on the resorption of calcium phosphate bone substitutes. Biomaterials. 25(17):3569–3582.2004; [PubMed: 15020131]
11. Bose S, Darsell J, Kintner M, Hosick H, Bandyopadhyay A. Pore size and pore volume effects on alumina and TCP ceramic scaffolds. Materials Science and Engineering: C. 23(4):479–486.2003;
12. Reffitt DM, Ogston N, Jugdaohsingh R, Cheung HFJ, Evans BAJ, Thompson RPH, Powell JJ, Hampson GN. Orthosilicic acid stimulates collagen type 1 synthesis and osteoblastic differentiation in human osteoblast-like cells in vitro. Bone. 32(2):127–135.2003; [PubMed: 12633784]
13. Gomes PS, Botelho C, Lopes MA, Santos JD, Fernandes MH. Effect of silicon-containing hydroxyapatite coatings on the human in vitro osteoblastic response. Bone. 44:S267.2009;
14. Fielding GA, Bandyopadhyay A, Bose S. Effects of silica and zinc oxide doping on mechanical and biological properties of 3D printed tricalcium phosphate tissue engineering scaffolds. Dental Materials. 28(2):113–122.2012; [PubMed: 22047943]
15. Roy M, Fielding GA, Bandyopadhyay A, Bose S. Effects of zinc and strontium substitution in tricalcium phosphate on osteoclast differentiation and resorption. Biomaterials science. 1(1):74–82.2013;
16. Kawamura H, Ito A, Miyakawa S, Layrolle P, Ojima K, Ichinose N, Tateishi T. Stimulatory effect of zinc-releasing calcium phosphate implant on bone formation in rabbit femora. Journal of Biomedical Materials Research: An Official Journal of The Society for Biomaterials, The Japanese Society for Biomaterials, and The Australian Society for Biomaterials and the Korean Society for Biomaterials. 50(2):184–190.2000;
17. Yuan H, De Bruijn JD, Li Y, Feng J, Yang Z, De Groot K, Zhang X. Bone formation induced by calcium phosphate ceramics in soft tissue of dogs: a comparative study between porous α-TCP and β-TCP. Journal of materials science: materials in medicine. 12(1):7–13.2001; [PubMed: 15348371]

18. LeGeros RZ. Properties of osteoconductive biomaterials: calcium phosphates. Clinical orthopaedics and related research. 395:81–98.2002;
19. Gaasbeek RD, Toonen HG, van Heerwaarden RJ, Buma P. Mechanism of bone incorporation of β-TCP bone substitute in open wedge tibial osteotomy in patients. Biomaterials. 26(33):6713–6719.2005; [PubMed: 15950278]
20. Bose S, Banerjee D, Robertson S, Vahabzadeh S. 2018Enhanced In Vivo Bone and Blood Vessel Formation by Iron Oxide and Silica Doped 3D Printed Tricalcium Phosphate Scaffolds. Annals of biomedical engineering. :1–13. [PubMed: 29019076]
21. Bose S, Tarafder S. Calcium phosphate ceramic systems in growth factor and drug delivery for bone tissue engineering: a review. Acta biomaterialia. 8(4):1401–1421.2012; [PubMed: 22127225]
22. Patel ZS, Yamamoto M, Ueda H, Tabata Y, Mikos AG. Biodegradable gelatin microparticles as delivery systems for the controlled release of bone morphogenetic protein-2. Acta biomaterialia. 4(5):1126–1138.2008; [PubMed: 18474452]
23. Suchanek W, Yashima M, Kakihana M, Yoshimura M. Hydroxyapatite ceramics with selected sintering additives. Biomaterials. 18(13):923–933.1997; [PubMed: 9199762]
24. Kanazawa T, Umegaki T, Yamashita K, Monma H, Hiramatsu T. Effects of additives on sintering and some properties of calcium phosphates with various Ca/P ratios. Journal of materials science. 26(2):417–422.1991;
25. Pichavant M. Effects of B and H 2 O on liquidus phase relations in the haplogranite system at l kbar. American Mineralogist. 72(11–12):1056–1070.1987;
26. Yamaguchi M. Role of nutritional zinc in the prevention of osteoporosis. Molecular and cellular biochemistry. 338(1–2):241–254.2010; [PubMed: 20035439]
27. Anavi Y, Avishai G, Calderon S, Allon DM. Bone remodeling in onlay beta-tricalcium phosphate and coral grafts to rat calvaria: microcomputerized tomography analysis. Journal of Oral Implantology. 37(4):379–386.2011; [PubMed: 20553149]
28. Hashizume M, Yamaguchi M. Effect of β-alanyl-L-histidinato zinc on differentiation of osteoblastic MC3T3-El cells: Increases in alkaline phosphatase activity and protein concentration. Molecular and cellular biochemistry. 131(1):19–24.1994; [PubMed: 8047061]
29. Li X, Sogo Y, Ito A, Mutsuzaki H, Ochiai N, Kobayashi T, Nakamura S, Yamashita K, LeGeros RZ. The optimum zinc content in set calcium phosphate cement for promoting bone formation in vivo. Materials Science and Engineering: C. 29(3):969–975.2009; [PubMed: 21461346]
30. Patel N, Best SM, Bonfield W, Gibson IR, Hing KA, Damien E, Revell PA. A comparative study on the in vivo behavior of hydroxyapatite and silicon substituted hydroxyapatite granules. Journal of Materials Science: Materials in Medicine. 13(12):1199–1206.2002; [PubMed: 15348666]
31. Camire CL, Jegou Saint-Jean S, Mochales C, Nevsten P, Wang JS, Lidgren L, McCarthy I, Ginebra MP. Material characterization and in vivo behavior of silicon substituted α-tricalcium phosphate cement. Journal of Biomedical Materials Research Part B: Applied Biomaterials. 76(2):424–431.2006;
32. Bandyopadhyay A, Shivaram A, Tarafder S, Sahasrabudhe H, Banerjee D, Bose S. In vivo response of laser processed porous titanium implants for load-bearing implants. Annals of biomedical engineering. 45(1):249–260.2017; [PubMed: 27307009]
33. Arinzeh TL, Peter SJ, Archambault MP, Van Den Bos C, Gordon S, Kraus K, Smith A, Kadiyala S. Allogeneic mesenchymal stem cells regenerate bone in a critical-sized canine segmental defect. JBJS. 85(10):1927–1935.2003;
34. Jiang T, Nukavarapu SP, Deng M, Jabbarzadeh E, Kofron MD, Doty SB, Abdel-Fattah WI, Laurencin CT. Chitosan–poly (lactide-co-glycolide) microsphere-based scaffolds for bone tissue engineering: In vitro degradation and in vivo bone regeneration studies. Acta biomaterialia. 6(9): 3457–3470.2010; [PubMed: 20307694]
35. Nandi SK, Ghosh SK, Kundu B, De DK, Basu D. Evaluation of new porous β-tri-calcium phosphate ceramic as bone substitute in goat model. Small Ruminant Research. 75(2):144–153.2008;
36. Gibson CJ, Thornton VF, Brown WAB. Incorporation of tetracycline into impeded and unimpeded mandibular incisors of the mouse. Calcified tissue research. 26(1):29–31.1978; [PubMed: 737550]

37. Dahners LE, Bos GD. Fluorescent tetracycline labeling as an aid to debridement of necrotic bone in the treatment of chronic osteomyelitis. Journal of orthopaedic trauma. 16(5):345–346.2002; [PubMed: 11972078]

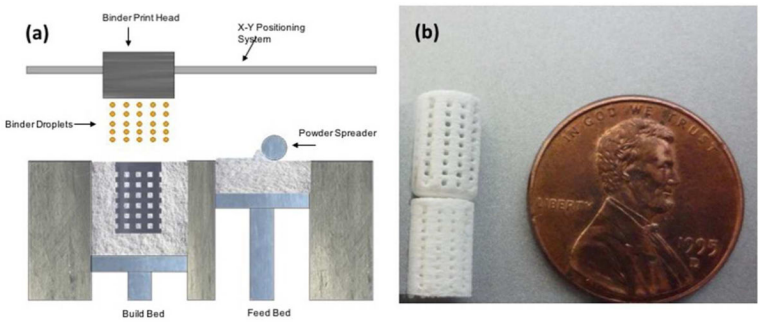

Figure 1.

(a) Schematic drawing representing the powder bed 3D printing process. (b) Photo showing fully processed green scaffolds (bottom: non-depowderized; top: depowderized), Square channels are oriented 0°/90° for subsequent layers.

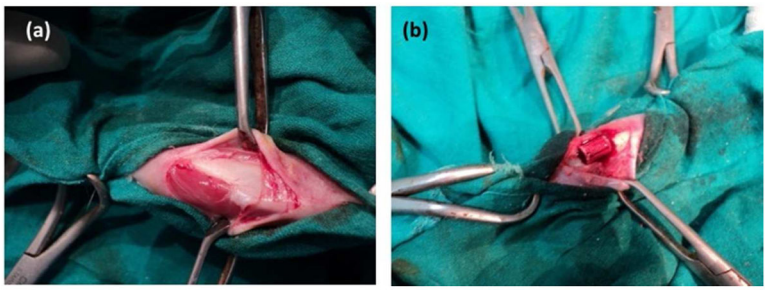

Figure 2.
Photograph showing a. Exposure of proximal tibia b. placement of implant in critical sized bone defect.

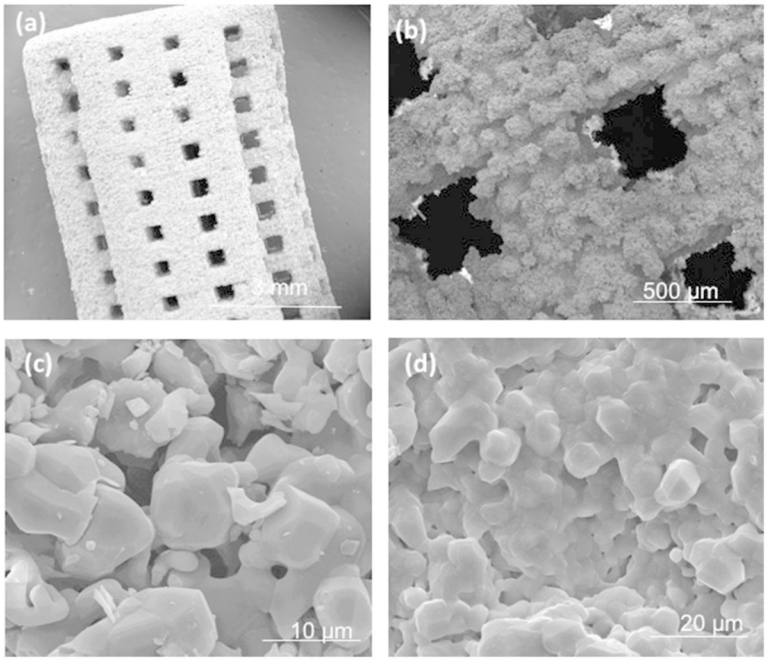

Figure 3.

Surface morphology of sintered scaffolds of (a–c) pure TCP scaffold at different magnifications and (b) SiO_2/ZnO doped scaffold depicting more liquid phase sintering evident from the glassy phase

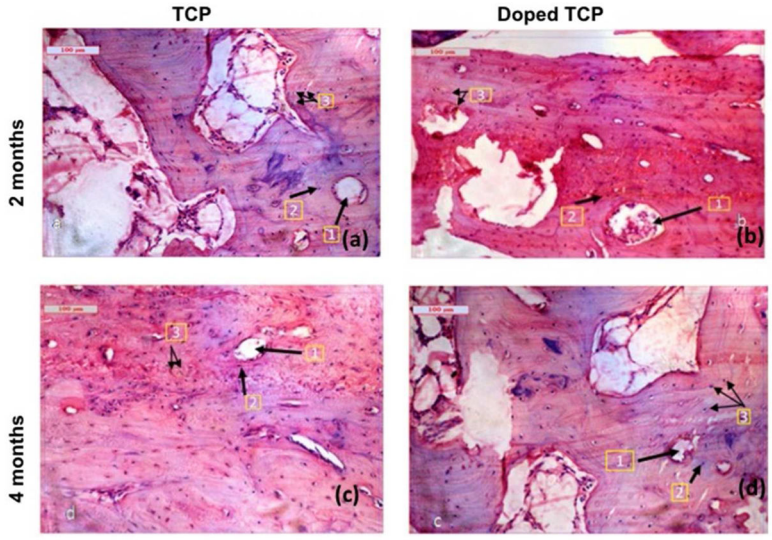

Figure 4.

Histological images depicting scaffolds implanted in the proximal tibia over the course of 120 days a. TCP-2months (1. Haversian canal 2. Lacunae 3. Osteoblast); b. Doped TCP-2months (1. Haversian canal 2. Lacunae 3. Angiogenesis); c. TCP-4months (1. Haversian canal 2. Lacunae 3. Osteoblast); d. Doped TCP-4 months (1. Haversian canal 2. Lacunae 3. Angiogenesis)

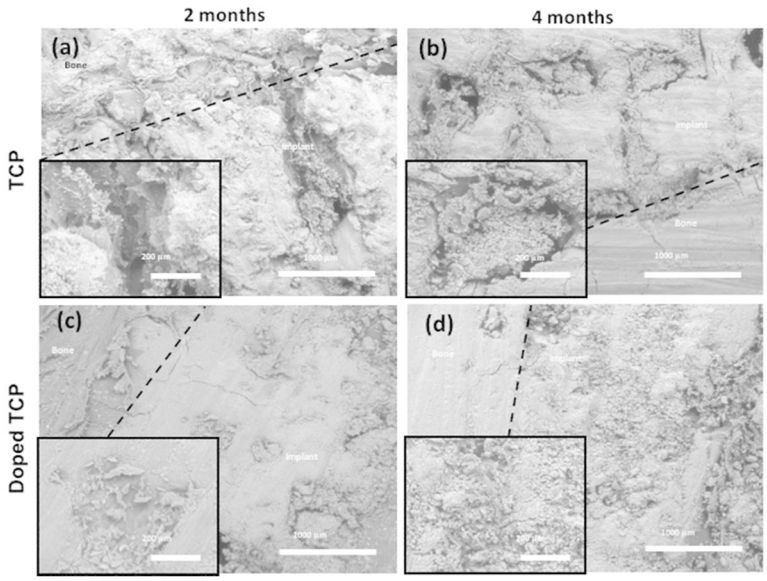

Figure 5.

SEM images of implanted pure TCP (top) and SiO_2/ZnO doped scaffolds (bottom) evaluated at 2 and 4 months after implantation. Insets show an increased magnification focusing on tissue ingrowth characteristics into the pores.

Figure 6.
X –ray images depicting scaffolds implanted in the proximal tibia over the course of 120 days.

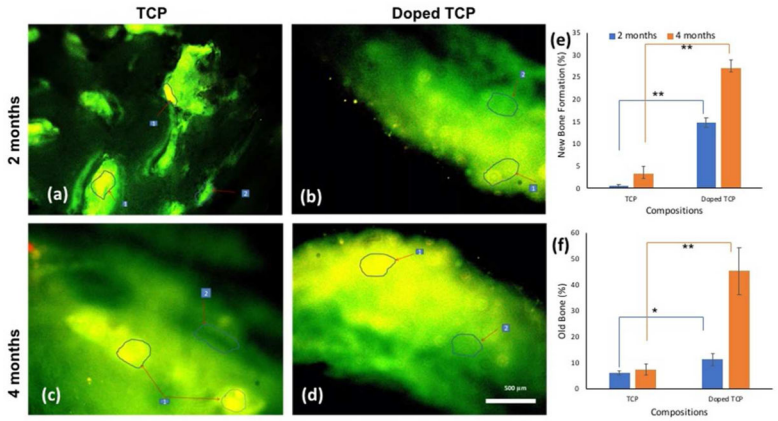

Figure 7.

Fluorochrome labeling images depicting scaffolds implanted in the proximal tibia over the course of 120 days. a. TCP 2 months' b. Doped TCP 2 months c. TCP 4 months d. Doped TCP 4 months. Areas marked with numbers depict the different osseous tissue zones (1. Golden yellow fluorescence- new bone 2. Sea green fluorescence- old bone). (e) and (f) show percentage old and new bone formation calculated from fluorochrome labeled micrographs using GNU Manipulation Program (GIMP). ** depicts extremely significant statistical relevance performed using Students' paired t tests (p values <0.0001) and * depicts significant relevance performed by Students' paired t-test as well (p value <0.05).